Adsorption (2019) 25:383–391
https://doi.org/10.1007/s10450-018-00002-4

New strategy of controlled, stepwise release from novel MBioF and its potential application for drug delivery systems

Adam Bieniek[1] · Marek Wiśniewski[1] · Katarzyna Roszek[2] · Paulina Bolibok[1] · Artur P. Terzyk[1] · Pilar Ferrer[3] · Ivan da Silva[4]

Received: 12 November 2018 / Revised: 19 December 2018 / Accepted: 21 December 2018 / Published online: 1 February 2019

Abstract
Metal organic structures have gained recently an interest in many fields. Among them, metal–biomolecule framework materials with amino acids applied as organic linkers have attracted the growing attention. An application of tailored metal–biomolecule frameworks, easily decomposing in an acidic and/or reductive environment in a steerable way, is reported here. From these biocompatible, non-porous, and nanostructured drug carrier systems, the desirable portion of drug could be released depending on the portion of acid, i.e. immediately and/or in a multi-step process due to a structure decomposition. The application of naturally occurring elements as cystine ensures full biocompatibility of the obtained system as well as its degradation products. Presented materials offer potential application in drug delivery systems.

Keywords Metal organic framework · MBioF · Stepwise release · Drug delivery system · Cystine · Cysteine · Sorafenib

1 Introduction

Metal organic frameworks (MOFs) have received a continuously increasing interest in different fields, among which adsorption (Coudert et al. 2013) and separation (Hamon et al. 2012) are the most popular. MOF adsorptive properties are medically applicable, and novel nanostructured materials tailored for the drug uptake/delivery are placed at the heart of modern treatment strategies (Zhang 2015; Dennis et al. 2016). However, MOFs application as drug carriers can be restricted due to the problems with the toxicity of components released during MOFs decomposition in tissues. Fortunately, various synthesis strategies of biocompatible MOF materials have been proposed. The first concept by Mantion et al. (2008), involves the use of so-called bioinspired MOF—metal–peptide frameworks (MPFs). Imaz et al. (2011) extended this idea to the development of so-called metal–biomolecule frameworks (MBioFs). In this general concept, different biomolecules (for example amino acids, peptides, nitrogen bases, etc.) have been incorporated into a MOF structure. This significantly solves the problem of toxicity. The review of recent progress in this field was published by Rojas et al. (2017).

The general assumption of the above mentioned concepts is that bioactive and/or neutral components should be metabolized (to run into a set of life-sustaining chemical transformations) after performing a specific task, without resulting in any undesirable symptoms. The simplest way is to use macroelements, i.e. the components already occurring and required in a body. In the case of an organic component, choosing the right one is much more complex due to the diversity of these structures. Thus, the optimal pre-selection is to choose the endogenous compounds (amino acid, peptides, sugars, etc.).

Among different drug delivery procedures, the pH-responsive method has been proposed in literature (Seib et al. 2013). For example, the ability of the silk nanoparticles to bind and release doxorubicin (DOX) with the use of

✉ Marek Wiśniewski
Marek.Wisniewski@umk.pl

[1] Physicochemistry of Carbon Materials Research Group, Faculty of Chemistry, Nicolaus Copernicus University in Toruń, ul. Gagarina 7, 87-100 Toruń, Poland

[2] Department of Biochemistry, Faculty of Biology and Environmental Protection, Nicolaus Copernicus University in Toruń, ul. Lwowska 1, 87-100 Toruń, Poland

[3] Diamond Light Source, Harwell Science and Innovation Campus, Chilton, Didcot OX11 0DE, UK

[4] Rutherford Appleton Laboratory, ISIS Neutron and Muon Source, Science and Technology Facilities Council, R3 UG.15, Harwell Campus, Didcot OX11 0QX, UK

pH as a stimulus was described by Seib et al. (2013) Likewise, Zou et al. (2017) used the effect of increasing DOX solubility at low pH values; however, the matrix remained undestroyed. The overall mechanism of the tested process was based on DOX weakly basic properties. Thus, its better solubility in acidic solutions was expected. The gradual insulin release from microcapsules prepared by a layer-by-layer deposition of poly(allylamine hydrochloride) and polyanions, such as poly(styrene sulfonate), poly(vinyl sulfate), and dextran sulfate was tested by Yoshida et al. (2015) The authors observed a faster release in basic environment than in acidic solutions and explained the phenomena by a different charge density of poly(allylamine hydrochloride) which is unstable in solutions of higher pH.

The above mentioned methods can be divided into two main groups reflecting the drugs (Seib et al. 2013; Zou et al. 2017; Yang et al. 2016; Tan et al. 2016) or matrix solubility (Yoshida et al. 2015; Gao et al. 2017). Among the latter, there are no studies that would report the matrix dissolution products to be fully biocompatible. Moreover, a matrix being both pH and redox sensitive has not been proposed in literature yet. The aim of this work is to fill this gap and to synthesize $Zn(Cys)_2$—an MBioF designed for a stepwise release of internalized molecules, including cytostatic agents.

2 Experiment

2.1 Materials

The used materials i.e. zinc chloride, cystine, methanol, potassium hydroxide, ascorbic acid, methylene blue, dimethyl sulfoxide were purchased from Sigma Aldrich; Sorafenib tosylate was purchased from Santa Cruz Biotechnologies.

2.2 Synthesis of $Zn(Cys)_2$

Cystine (2,4 g) and potassium hydroxide (1.69 g) were dissolved in 150 ml solution of MeOH and H_2O 2:1 (v:v) mixture. Separately, zinc chloride was dissolved in 150 ml of a similar MeOH/H_2O solution. Both solutions were mixed and stirred for 1 h at room temperature. The resulting precipitate was washed several times with methanol and finally with deionized water. The obtained precipitate was centrifuged and thus gained white powder was dried at 50 °C in a vacuum oven (24 h).

2.3 Sorafenib (SOR)/Methylene blue (MB)—adsorption and release

Mass of 20 mg of $Zn(Cys)_2$ was added to the solution of MB in DMF (c = 0.002 mol/l) and shacked for 24 h (200 rpm). Next, the mixture was centrifuged and the precipitate was washed with H_2O. The obtained product was dried in vacuum oven at 50 °C for 24 h. In the case of SOR, 50 mg of $Zn(Cys)_2$ was added to the solution containing DMSO solution of SOR-tosylate (c = 0.18 mol/l) and shaken for 24 h (200 rpm). Next, the precipitate was filtered through a membrane filter (450 nm) and rinsed with 100 ml water, 20 ml DMSO, and 100 ml of water. The obtained product was dried in the vacuum oven at 50 °C for 24 h. MB and SOR adsorption values were calculated from the difference in concentrations, and they were the same as calculated from the concentrations of the both solutions after acid-induced release.

To study the MB/SOR release, known mass of MB and SOR adsorbed on $Zn(Cys)_2$ was introduced to a thermostated container with distilled water. To observe the acid-induced desorption 0.1 M HCl was used. Moreover in the case of MBioF with adsorbed MB, 0.1 M ascorbic acid (AA) was also applied, due to its biocompatibility. Before and after administering of acids, the concentration of MB/SOR was monitored under continuous stirring of the mixture at the constant temperature (295 K) using Jasco V-660 UV–vis spectrophotometer (JASCO, Japan). The spectra during release were also recorded for MB (550–700 nm) and SOR (239–287 nm) and no changes in spectra were observed.

2.4 Material characterization

The produced $Zn(Cys)_2$ was characterized with scanning electron microscopy (SEM), using a Quanta 3D FEG (EHT = 30 kV) instrument. The powdered samples were placed onto carbon tabs attached to aluminum SEM stubs. Bulk powder MBioFs were characterized with PXRD using a Philips XPERT Pro diffractometer with CuKα1 radiation. The Fourier transform infrared spectra (FTIR) measurements were accomplished by a Bruker Vertex 70 infrared spectrophotometer using Platinum diamond ATR techniques in the frequency range 60–4000 cm^{-1}. The nonpolarized Raman scattering spectra of tested structures were investigated in the spectral range of 60–4500 cm^{-1}. The Raman spectra were recorded in the backscattering geometry using a SENTERRA micro-Raman system. As an excitation light, we used a green laser operating at 532 nm. The laser beam was tightly focused on the sample surface through a 50x microscope objective. The position of the microscope objective with respect to the sample was piezoelectrically controlled (XY position). To prevent any damage of the sample, excitation power was fixed at 2 mW. The resolution was 4 cm^{-1}, CCD temperature 223 K, laser spot diameter—2.0 µm, and total integration time 100 s (50 × 2 s), were used. Nitrogen adsorption–desorption isotherms were measured using an ASAP 2010 volumetric adsorption analyzer from Micromeritics (Norcross, GA, USA) at liquid

nitrogen temperature (77 K) in the relative pressure range from about 10^{-6} up to 0.999. Before the measurements, the samples were outgassed for at least 2 h at a temperature of 373 K. Thermogravimetric measurements were performed in N_2 or air atmosphere using a Simultaneous TGA-DTA (TA Instruments, type SDT 2960) thermal analyzer in the temperature range of 293–1273 K. The heating rate was 10 K min^{-1}. The elemental analysis was performed using a Vario MACRO CHN apparatus from ELEMENTAR Analysensysteme GmbH.

2.4.1 Cytotoxicity test

3T3 mouse embryonic fibroblasts were purchased from Sigma–Aldrich. Cells were grown in a low-glucose DMEM medium containing 2 mM L-glutamine and supplemented with 10% FBS, at 37 °C in a CO_2 incubator with 5% of CO_2. A volume of 25 µl containing 5×10^4 cells was seeded to each well of a 12-well plate 24 h before the experiment was started. MBioOFs samples were added to the growing 3T3 cells at the final concentrations of 1, 10, 25, 50, and 100 µg ml^{-1} and incubated for the next 24 h. Subsequently, the MTT test based on the ability to reduce 3-(4,5-dimethylthiazol-2-yl)-2,5-diphenyltetrazolium bromide (MTT) by mitochondrial dehydrogenases was performed in triplicate for assessing cell metabolic activity and viability. The medium with $Zn(Cys)_2$ was discarded and MTT solution (0.5 mg ml^{-1} concentration) was added to the wells with 3T3 cells after 24 h incubation. After 10 min incubation, the solution was discarded and formazan crystals were dissolved in 2 ml DMSO. Absorbance (570 nm) was measured spectrophotometrically. The viability of cells growing without $Zn(Cys)_2$ was taken as a 100% control.

2.4.2 Statistical analysis

The experiments were conducted at least three times in triplicate and qualitatively identical results were obtained. The presented results are representative for three tested series of experiments.

2.4.3 Ab-initio calculations

To explain the mechanism of MB and SOR adsorption–desorption phenomena, the calculations of interactions energies have been performed (via GAUSSIAN 03) at B3LYP level of DFT using 6-31G(d,p) basis sets. (Frish et al. 2003). Follow Young the Basis Set Superposition Error (BSSE) has been taken into account during the energy calculations. Due to the huge size of surface in a real material, as well as to make the DFT calculations possible the studied structures should be small. Thus only a part of a $Zn(Cys)_2$ surface has been analyzed. The same procedure has been widely applied, for example during the DFT studies of carbon nanotubes (Wiśniewski et al. 2010) and/or during the calculations of interaction energy between the MB and single-stranded DNA fragments (Ortiz et al. 2011).

3 Results and discussion

The new application of nanostructural, non-porous $Zn(Cys)_2$ is described in this work. The data collected in Fig. 1 prove that the obtained material possesses a mesoporous structure with the crystal size below 50 nm. The XRD results collected in Fig. 1b show sharp signals and the lack of an amorphous phase, which confirms the crystallinity of studied MBioF. The XRD pattern corresponds completely to the one proposed by Ferrer et al. (2014). The low temperature N_2 adsorption–desorption isotherm of tested material is of type IV (Fig. 1c), and the pore size distribution (inset in Fig. 1c) reveals the presence of mesopores.

The careful analysis of the isotherm leads to the conclusion that the studied material is "flat-surfaced", having the BET specific surface area equal to 96 m^2/g. The absence of pores in the structure has been also confirmed by the application of the Bhattacharya-Gubbins method (Bhattacharya and Gubbins 2006) using, for the studied MBioF, the OPLS-AA force field parameters taken from the Open MM simulation toolkit (Friedrichs et al. 2009).

The shape of very small hysteresis loop, together with the results of the Bhattacharya-Gubbins method, lead to the conclusion about the presence of negligibly small amount of large mesopores (so called "secondary porosity" between crystals, with the average pore diameter equal to c.a. 20 nm). Moreover, since in mesopores the overlapping of the potential energy from opposite walls does not occur, the mesopores in the studied MBioF material behave as a flat surface, especially during a low-coverage adsorption process.

Cytotoxicity evaluation (Fig. 1d) indicates that the tested material does not significantly change 3T3 fibroblasts viability. Based on the MTT test results, one can conclude that the material is nontoxic in a very wide concentrations range. Therefore, the structure can be treated as biocompatible, while its EC_{50} for 3T3 cell line is over 100 mg/l.

The TG results presented in Fig. 2 show that thermal stability of the obtained $Zn(Cys)_2$ is strongly related to the stability of the organic linker ($(Cys)_2$). The thermograms were taken under air and N_2 atmosphere and compared in terms of their weight losses against temperature. In all cases the results show one sharp degradation starting with initial degradation temperature of 230 and 250 °C for cystine and MBioF respectively, and continued up to 650 °C in air, and up to 1000 under N_2 with degradation weight loss of ca. 98% for cystine, and ca. 68% under N_2 of its initial weight.

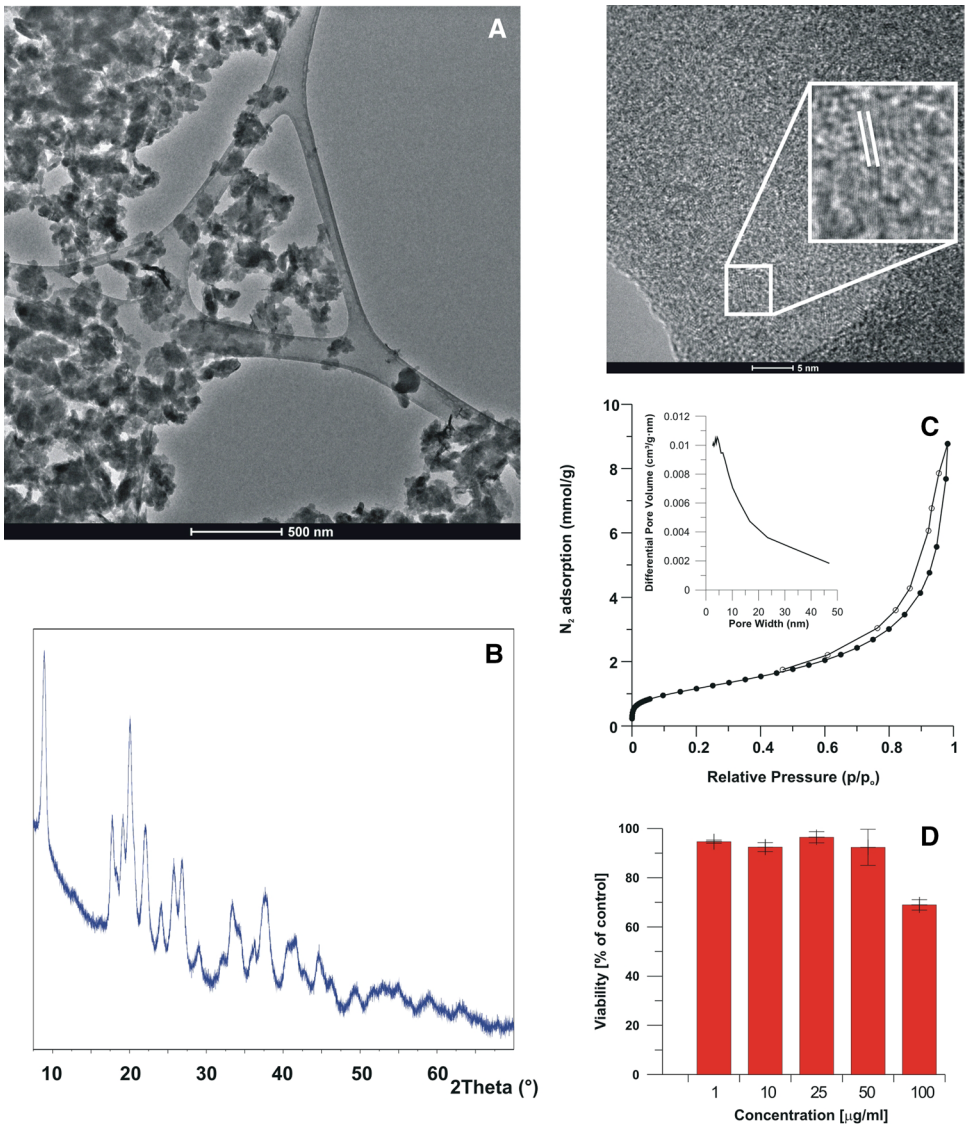

Fig. 1 Physicochemical characterization of obtained $Zn(Cys)_2$. **a** HRTEM picture; **b** XRD pattern, **c** low temperature N_2 adsorption (filled symbols)-desorption (open symbols) isotherm, with the pore size distribution (inset) and **d** cytotoxicity of produced MBioF

A lower degree of $Zn(Cys)_2$ decomposition, when compared to $(Cys)_2$, is caused by the presence of the metallic node. The elemental analysis for C, H and N, averaged from three measurements are equal: C, 23.67 (23.73); H, 3.483 (3.29); N, 8.754 (9.22) (% of the theoretical values are given in parentheses). The above, together with EDX data confirm the stoichiometry of the structure, i.e. $Zn(Cys)_2$.

Interestingly, the decomposition of organic linker, i.e. cystine, is shifted about 50 °C to higher temperatures after incorporation into the MBioF structure. This observation is in line with the data reported by other authors for different MOFs and means that chelation and heterocyclic ring formation occurs (Chaudhary et al. 2016).

The characteristic signals for amino acids hydrogen bonds are visible in the FTIR spectrum of $(Cys)_2$ as a broad and mutually overlapping band in the OH/NH stretching spectral range of 3300 up to 2300 cm^{-1} as well as in the bending range ~ 1500 cm^{-1} (Fig. 3). Interestingly, those bands are almost invisible in the Raman spectrum. These phenomena can be explained by the fact that for hydrogen bonds, during normal vibration, causing periodic changes in the structure of the atomic cores, the force of electron binding in the molecule does not change. Therefore, the polarizability cannot be a function of the coordinates of the normal vibration. In contrast, the low polarity and high polarizability of CH bonds causes a low FTIR intensity of ν(CH) to increase in the Raman spectrum.

The formation of the MBioF causes the structure to lose the hydrogen bonds revealing the ν(NH) asymmetric and symmetric signals at 3350 and 3250 cm^{-1} and δ(NH_2) at 1564 cm^{-1}, respectively. Note that there are no ν(OH) in the IR as well as in the Raman spectrum meaning that in the obtained MBioF carboxyl groups are involved in the metal ion nodes.

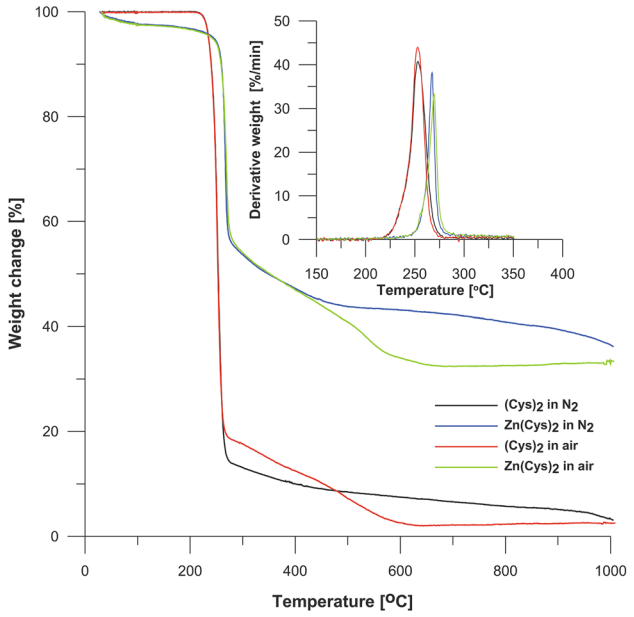

Fig. 2 Thermal stability of $(Cys)_2$ and obtained $Zn(Cys)_2$ in air and in nitrogen atmosphere

The absence of ν(OH) as well as the presence of sole and isolated ν(NH) indicates a stiffness of the $-NH_2$ group due to H_2N–Zn bonding. The hypothesis is completely in line with the one proposed by Ferrer et al. (2014) for the MBioF formation through O (of COO^- group)–Zn^{2+}–N (of NH_2 group) bonding.

The formation of metal-cystine bonds is visible also as the appearance of the band at 915 cm^{-1} and ~ 15 cm^{-1} blue-shift of ν(SS) signal in the Raman spectrum. The former is responsible for the C–O–Zn bonds formation. It is much higher in intensity in the Raman than in the FTIR, contrary to the ν(C–O) from COOH groups visible only in FTIR at 872 cm^{-1}. The S–S Raman signal will be used further to characterize the SS bond in $(Cys)_2$ or in the $Zn(Cys)_2$ structure. Note that neither in the Raman nor in the FTIR spectra the characteristic signals for $ZnO/Zn(OH)_2$ exist.

Methylene blue (MB) is a photosensitizer used in photodynamic therapy to treat colorectal cancer tumors and *Leishmania* infections. (Bruschi et al. 2018) Besides that, MB is very often used as a model drug to investigate the loading and release ability of the synthesized drug delivery systems (Ding et al. 2012).

On the other hand, Sorafenib (SOR) is the second generation anticancer drug. The drug is a multi-kinase and angiogenesis inhibitor efficacious for hepatocellular carcinoma treatment. Although SOR is an accepted drug, its administration is associated with significant side effects.

In order to avoid different side effects and inherent toxicities of used drugs, there are still attempts to use small cytostatic doses. In this field new possibilities are offered by so called passive drug targeting and delivery, involving the fabrication of biocompatible nanoparticles and the conjugation of drugs with such entities (Werengowska-Ciecwierz et al. 2014).

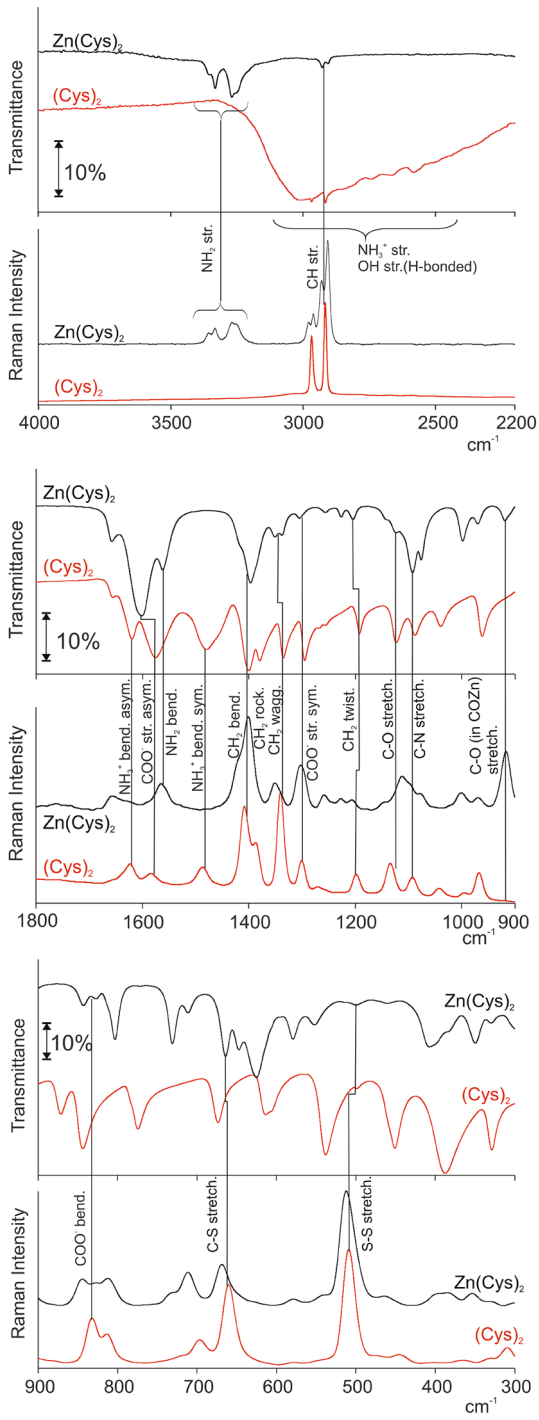

Fig. 3 Comparison of room temperature vibrational spectra for $Zn(Cys)_2$ and $(Cys)_2$. The vertical lines show the correspondence between the Raman and FTIR bands

Figure 4 shows that in an aqueous solution, MB and/or SOR are desorbed from the structure very negligibly. In contrast, a stepwise increase in concentration of the both compounds is induced by the addition of HCl and/or ascorbic acid (AA). It is also extremely important that after the addition of 150 µL HCl or 100 µL AA solution to the reaction vessel, the MB concentration immediately rises to the maximal level.

For SOR the typical adsorption–desorption studies are rarely met in literature (Heidarinasa et al. 2016; Zheng et al. 2018) thus the mechanism of releasing is not fully understood. In order to shed some light to observed phenomena, i.e. an acid-induced stepwise desorption from the MBioF surface, the results from simple model in *ab-initio* calculations as well as Raman spectroscopy data have been collected. The interaction energies are presented in Table 1. The results show that the largest absolute energy value is observed for MB adsorbed on $Zn(Cys)_2$ modxelled surface and SOR adsorbed on $Zn(Cys)_2$. In contrast, interactions between H_2O and MB as well as H_2O and SOR exhibit much lower energy values. The harnessing of even such simple approach explains the very slow desorption process in pure water (see Figs. 4 and 5).

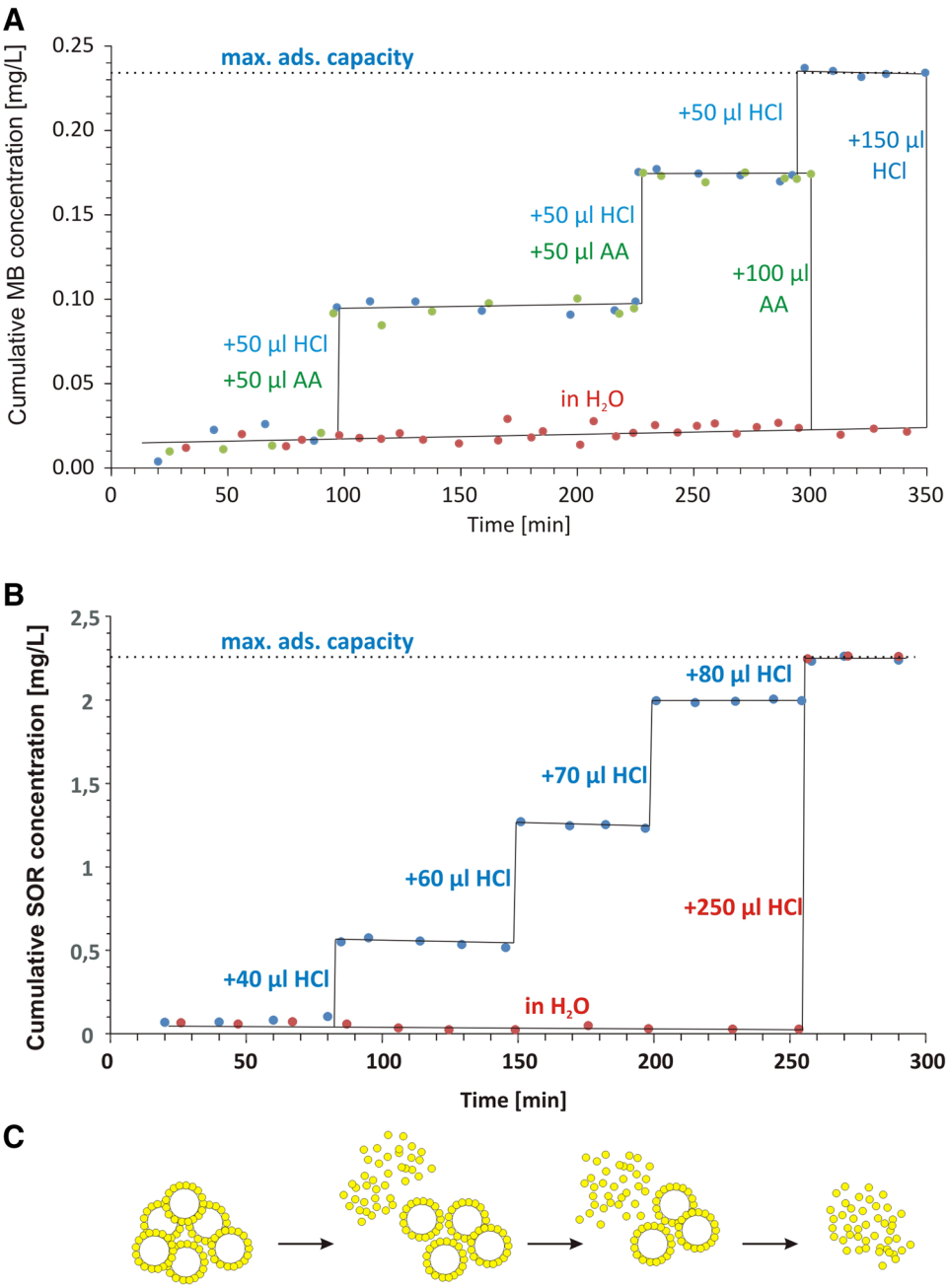

Fig. 4 MB (**a**) and SOR (**b**) stepwise release from the $Zn(Cys)_2$ MBioF. Red dots indicate the concentration of MB or SOR in water, respectively. Blue and green dots represent concentrations after the addition of the destroying agent (i.e. HCl or AA) to the $Zn(Cys)_2$ MBioF; **c** schematic representation of observed phenomena. (Color figure online)

Table 1 DFT-calculated values of the interaction energy between water, MB, SOR and $Zn(Cys)_2$

System	Interaction energy (kJ/mole)
$H_2O + MB$	− 17.13
$H_2O + SOR$	− 26.64
$H_2O + Zn(Cys)_2$	− 54.54
$MB + Zn(Cys)_2$	− 86.44
$SOR + Zn(Cys)_2$	− 57.19

After the addition of acids to solutions the destruction of the matrix starts. Due to relatively high absolute value of H_2O and $Zn(Cys)_2$ interaction energy, the desorption of MB and SOR occurs.

In Fig. 6 one can observe that cystine as well as cysteine are formed as the products obtained during $Zn(Cys)_2$ treatment with HCl and AA. The spectra reveal the band at 915 cm^{-1} disappearing and some rearrangement in the region at ~650–750 cm^{-1} as well as the red-shifting of the ν(S–S) signal. It is obvious that the studied MBioF after HCl or AA addition decomposes into the $(Cys)_2$ which forms Cys in the solution, according to the scheme:

$$Zn(Cys)_2 + 2H^+ \rightarrow Zn^{2+} + (Cys)_2$$

$$(Cys)_2 + AA \rightarrow 2Cys + DHA$$

In the literature, there are examples of doxorubicin (DOX) drug delivery systems being pH dependent. (Seib et al. 2013; Zou et al. 2017; Yoshida et al. 2015). However the stepwise release after lowering the pH value results from unique properties of DOX itself and cannot be applied to other cytostatic drugs. Described here drug delivery system is universal and does not depend on the drug properties.

The method proposed in this work utilizes two sensitive points of synthetized MBioF: (i) for acidic environment - the metal node, and (ii) for reductive agents—the S–S bond in cystine. Therefore, exposed to acidic or reductive environment, the new MBioF—based drug delivery system decomposes immediately and releases the internalized active agent. This new proposal, in comparison to other drug delivery systems (Werengowska-Ciecwierz et al. 2014), offers three major advantages. The first one is the biocompatibility of any particular element of the system at every single step of the delivery process. The second advantage is that the process of an active substance release is based on a chemical reaction. What is important, this reaction can be controlled

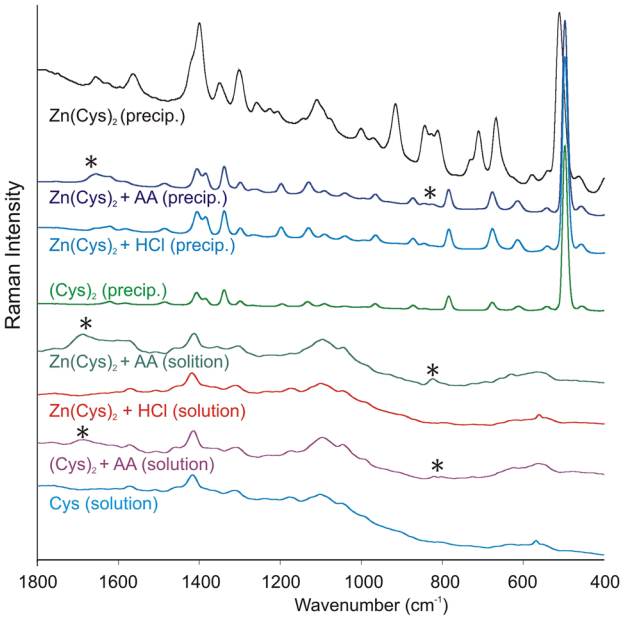

Fig. 6 The Raman spectra of $Zn(Cys)_2$ products resulted after treatment with HCl and AA in comparison with $(Cys)_2$ and Cys spectra with the scheme of the overall process. Asterisks denote the remaining AA

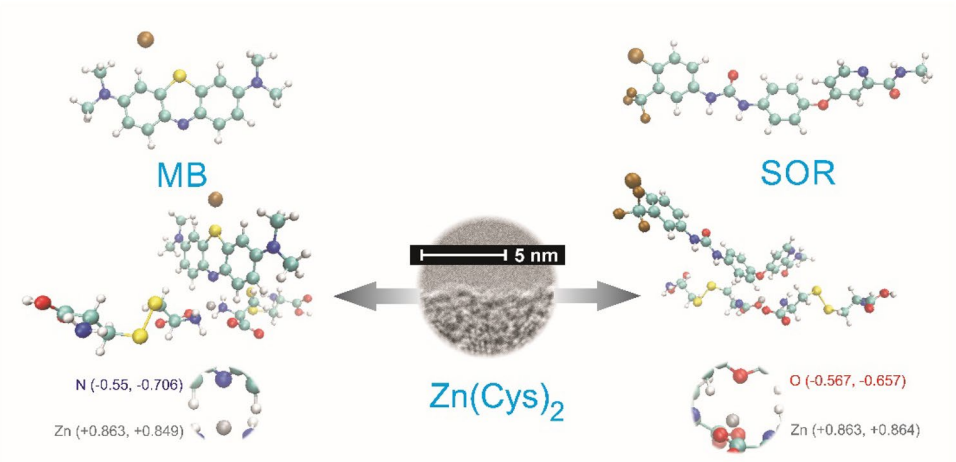

Fig. 5 The equilibrated conformations of isolated molecules (top row) and the molecules interacting with the part of the CP surface. Bottom row shows magnified region of interaction. In the parentheses the charges of interacted atoms i.e. O, Zn, and N before and after equilibration are presented

quantitatively; therefore, any particular dose of a drug can be released. Finally, velocity of the delivery process does not depend on the rate of physical desorption because chemical MBioF decomposition is much faster.

4 Conclusions

The MBioF material was characterized using scanning electron microscopy (SEM), powder X-ray diffraction (PXRD), Fourier Transform Infrared (FTIR) and Raman spectroscopy, low-temperature nitrogen adsorption, elemental analysis, and thermogravimetric (TG) measurements in air and in nitrogen atmosphere. Additionally, cytotoxicity tests were performed. Methylene blue (MB) and Sorafenib (SOR) were used as model therapeutic agents for drug release experiments.

In conclusion, newly synthesized MBioF with the use of naturally occurring, and thus, biocompatible elements is described in this work. The analyses confirm its nanostructural, nonporous, and nontoxic nature. The possibility of the internalized active agent stepwise release driven by acidic or reductive environment is proved experimentally. The new MBioF-based drug delivery system can decompose immediately releasing the maximal available dose of a therapeutically active molecule incorporated in the structure. On the other hand, a multi-step, fully controllable desorption of smaller doses is also possible, maximizing therefore a potential activity of the therapeutic agent (for example anticancer drug SOR) tailored to a patient's needs. Thus, the proposed MBioF can find a potential application during tailoring the new drug delivery systems with fully steerable properties.

Acknowledgements We gratefully acknowledge financial support by the Polish National Science Centre (NCN) Grant OPUS 9 No. 2015/17/B/ST5/01446.

References

Bhattacharya, S., Gubbins, K.E.: Fast method for computing pore size distributions of model materials. Langmuir. **29**, 7726–7731 (2006)

Bruschi, M.L., Junqueira, M.V., Borghi-Pangoni, F.B., Yu, T., Andrews, G.P., Jones, D.S.: Investigation of methylene blue release from functional polymeric systems using dielectric analysis. Curr. Drug Deliv. **15**, 64–76 (2018)

Chaudhary, R.G., Ali, P., Gandhare, N.V., Tanna, J.A., Juneja, H.D.: Thermal decomposition kinetics of some transition metal coordination polymers of fumaroyl bis (paramethoxyphenylcarbamide) using DTG/DTA techniques. Arab. J. Chem. (2016). https://doi.org/10.1016/j.arabjc.2016.03.008

Coudert, F.X., Boutin, A., Fuchs, A.H., Neimark, A.V.: Adsorption deformation and structural transitions in metal–organic frameworks: from the unit cell to the crystal. J. Phys. Chem. Lett. **4**, 3198–3205 (2013)

Dennis, A.M., Delehanty, J.B., Medintz, I.L.: Emerging physicochemical phenomena along with new opportunities at the biomolecular-nanoparticle interface. J. Phys. Chem. Lett. **7**, 2139–2150 (2016)

Ding, C., Xu, S., Wang, J., Liu, Y., Hu, X., Chen, P., Feng, S.: Controlled loading and release of methylene blue from LbL polyurethane/poly(acrylic acid) film. Polym. Adv. Technol. **23**, 1283–1286 (2012)

Ferrer, P., da Silva, I., Rubio-Zuazo, J., Castro, G.R.: Synthesis and crystal structure of the novel metal organic framework $Zn(C_3H_5NO_2S)_2$. Powder Diffr. **29**, 366–370 (2014)

Friedrichs, M.S., Eastman, P., Vaidyanathan, V., Houston, M., LeGrand, S., Beberg, A.L., Ensign, D.L., Bruns, C.M., Pande, V.S.: Accelerating molecular dynamic simulation on graphics processing units. J. Comput. Chem. **30**, 864–872 (2009)

Frisch, M.J., et al.: GAUSSIAN 03, Revision D.01. Gaussian, Inc., Pittsburgh (2003)

Gao, X., Cui, R., Zhang, M., Liu, Z.: Metal-organic framework nanosheets that exhibit pH-controlled drug release. Mater. Lett. **15**, 217–220 (2017)

Hamon, L., Heymans, N., Llewellyn, P.L., Guillerm, V., Ghoufi, A., Vaesen, S., Maurin, G., Serre, C., Weireld, G.D., Pirngruber, G.D.: Separation of CO_2–CH_4 mixtures in the mesoporous MIL-100(Cr) MOF: experimental and modelling approaches. Dalton Trans. **41**, 4052–4059 (2012)

Heidarinasa, A., Panahi, H.A., Faramarzi, M., Farjadian, F.: Synthesis of thermosensitive magnetic nanocarrier for controlled sorafenib delivery. Mater. Sci. Engn. C. **67**, 42–50 (2016)

Imaz, I., Rubio-Martínez, M., An, J., Sole-Font, I., Rosi, N.L., Maspoch, D.: Metal-biomolecule frameworks (MBioFs). Chem. Commun. **47**, 7287–7302 (2011)

Mantion, A., Massüger, L., Rabu, P., Palivan, C., McCusker, L.B., Taubert, A.: Metal-peptide frameworks (MPFs): "bioinspired" metal organic frameworks. J. Am. Chem. Soc. **130**, 2517–2526 (2008)

Ortiz, A.M., Fragoso, A., Ortiz, P.J., O'Sullivan, C.K.: Elucidation of the mechanism of single-stranded DNA interaction with methylene blue: a spectroscopic approach. J. Photochem. Photobiol. A: Chemistry. **218**, 26–32 (2011)

Rojas, S., Devic, T., Horcajada, P.: Metal organic frameworks based on bioactive components. J. Mater. Chem. B. **5**, 2560–2573 (2017)

Seib, F.P., Jones, G.T., Rnjak-Kovacina, J., Lin, Y., Kaplan, D.L.: pH-Dependent anticancer drug release from silk nanoparticles. Adv. Healthcare Mater. **2**, 1606–1611 (2013)

Tan, S.Y., Ang, C.Y., Mahmood, A., Qu, Q., Li, P., Zou, R., Zhao, Y.: Doxorubicin-loaded metal–organic gels for pH and glutathione dual-responsive release. ChemNanoMat **2**, 504–508 (2016)

Werengowska-Ciećwierz, K., Wiśniewski, M., Terzyk, A.P., Gurtowska, N., Olkowska, J., Kloskowski, T., Drewa, T.A., Kiełkowska, U., Drużyński, S.: Nanotube—mediated efficiency of cisplatin anticancer therapy. Carbon. **70**, 46–58 (2014)

Wiśniewski, M., Rychlicki, G., Arcimowicz, A.: Experimental and theoretical estimations of the polar force contributions to the heat of immersion of carbon nanotubes. Chem. Phys. Lett. **485**, 331–334 (2010)

Yang, Y., Hu, Q., Zhang, Q., Jiang, K., Lin, W., Yang, Y., Cui, Y., Qian, G.: A large capacity cationic metal-organic framework nanocarrier for physiological pH responsive drug delivery. Mol. Pharm. **13**, 2782–2786 (2016)

Yoshida, K., Ono, T., Kashiwagi, Y., Takahashi, S., Sato, K., Anzai, J.: pH-Dependent release of insulin from layer-by-layer-deposited polyelectrolyte microcapsules. Polymers **7**, 1269–1278 (2015)

Zhang, J.Z.: Some interesting properties and promising applications of nanostructured materials. J. Phys. Chem. Lett. **6**, 4429–4430 (2015)

Zheng, G.R., Zhao, R.R., Xu, A.X., Shen, Z.C., Chen, X., Shao, J.W.: Co-delivery of sorafenib and siVEGF based on mesoporous silica

nanoparticles for ASGPR mediated targeted HCC therapy. Eur. J. Pharm. Sci. **111**, 492–502 (2018)
Zou, Z., Li, S., He, D., He, X., Wang, K., Li, L., Yang, X., Li, H.: A versatile stimulus-responsive metal–organic framework for size/morphology tunable hollow mesoporous silica and pH-triggered drug delivery. J. Mater. Chem. B. **5**, 2126–2132 (2017)